JOURNAL OF MATERIALS SCIENCE **38** (2003) 499–506

An impedance spectroscopy study of oxide films formed during high temperature oxidation of an austenitic stainless steel

S.-H. SONG*, P. XIAO*,‡
Materials Group, Department of Mechanical Engineering, Brunel University, Uxbridge, Middlesex UB8 3PH, UK
E-mail: Ping.Xiao@man.ac.uk

Impedance spectroscopy has been used to study an oxide film formed on an AISI304 austentic stainless steel by oxidation at 800°C for 200 h. Impedance spectra of the oxide film clearly showed two semicircles, which correspond to two independent oxide layers present in the oxide film. The oxide film was also examined by using scanning electron microscopy (SEM), X-ray photoelectron spectroscopy (XPS) and X-ray diffraction (XRD). Although it was difficult to identify the two phases in the oxide film using SEM, XRD showed the presence of Cr_2O_3 and $MnCr_2O_4$. In addition, surface analysis of the oxide film using XPS showed the presence of $MnCr_2O_4$. By comparing the relaxation frequencies of Cr_2O_3 and $MnCr_2O_4$ with those of the two semicircles, it is identified that the semicircles in the impedance spectra correspond to Cr_2O_3 and $MnCr_2O_4$. Furthermore, the electrical properties of both Cr_2O_3 and $MnCr_2O_4$ in the oxide film have been determined by impedance measurements, indicating that the chromia layer is apparently thicker than the spinel layer.

1. Introduction

High temperature oxidation is a common process for metallic materials. For this reason, heat-resistant alloys such as stainless steels and Ni-base superalloys have been developed and widely employed in engineering practice [1, 2]. The mechanism for these materials to be oxidation-resistant is the formation of a protective oxide film, such as Cr_2O_3, SiO_2 or Al_2O_3, on their surfaces during their high temperature exposure [3, 4]. The protective ability of an oxide film is dependent on its ability to reduce the rate of oxidation reactions by acting as a diffusion barrier between the metallic material and the oxidising environment. As a result, oxide films have a key function in high temperature applications of metallic materials.

The oxide film formed due to high temperature oxidation of steels usually has several oxide layers. The protective capability of the oxide film depends mainly on the nature of the oxide layers. Therefore, it is important to characterise their microstructure and electrical properties. A number of techniques, such as weight gain measurements, electron microscopy, X-ray diffraction and surface analysis, have been employed to evaluate such a film [3, 5–7]. However, it is difficult to use these techniques to distinguish individual oxide layers and examine the continuity of the oxide layers. In addition, these techniques require destructive preparation of specimens for analysis. Impedance spectroscopy is a simple, effective and non-destructive technique, which can be used to examine the oxide film [8]. It can be used to distinguish and determine the electrical and dielectric properties of different oxide layers. All these data are useful in studying oxidation mechanisms.

Austenitic stainless steels are widely used heat-resistant steels. During high temperature oxidation, an oxide film containing several oxide layers is usually formed on the steels [3]. The nature of these individual layers plays an important part in its oxidation resistance. The addition of chromium to high temperature alloys has often been used for producing a protective oxide film [3]. With a low concentration of Cr present in steels [3], a spinel layer $FeFe_{(2-x)}Cr_xO_4$ ($x = 0$-2) is usually formed between the iron oxides and the metal substrate. The increase in the Cr content decreases the Fe cation diffusion through the spinel and thus lowers the oxidation rate. Further increase in the Cr content may lead to the formation of a Cr_2O_3 layer at the iron oxide/metal phase boundary. If the Cr content were sufficiently high, the formation of the Fe oxide layers (Fe_2O_3, Fe_3O_4 and FeO) would be suppressed. Previous studies on the oxidation of Mn-bearing Cr steels below 900°C [9–11] indicates that when the Cr content is between 17 wt% and 25 wt% the oxide film consists of an $MnCr_2O_4$ spinel and Cr_2O_3, where the spinel

Present Address: Manchester Materials Science Centre, University of Manchester, Grosvenor Street, Manchester M1 7HS, UK.
‡Author to whom all correspondence should be addressed.

may contain some Fe. If silicon is present in a high Cr steel, an SiO_2 layer may be formed underneath the outer $MnCr_2O_4$ spinel and Cr_2O_3 layers [3]. Pan *et al.* [12] recently investigated the oxidation behaviour of an AISI 304 austenitic stainless steel using impedance spectroscopy. In their work, the steel was oxidised in air at 800°C and the impedance measurements were performed at room temperature with an electrolyte solution (0.1 M Na_2SO_4) contacting the oxide surface. Their results demonstrate that in addition to an outer porous $MnCr_2O_4$ spinel layer and an inner dense Cr_2O_3 layer there is a thin amorphous SiO_2 layer formed between the Cr_2O_3 layer and the steel substrate. Recently, Botella *et al.* [13] also investigated high-temperature oxidation of the same type of steel doped with some Cu by means of X-ray diffraction, scanning electron microscopy together with microanalysis. In their work, the material was oxidised in air at 700°C and similar results as above were found except for faster oxidation rates.

In the presnt work, impedance spectroscopy (IS) has been employed to evaluate the oxide film formed on an austenitic stainless steel in air at 800°C. To avoid the electrolyte solution penetration into the oxide film and to reduce the moisture effect on its electrical properties, the impedance measurements have been conducted at temperatures above 100°C with a platinum foil as the conuter electrode, which directly contacted the oxide surface without an electrolyte solution involved. In addition, the impedance results have further been supported by scanning electron microscopy (SEM), X-ray photoelectron spectroscopy (XPS) and X-ray diffraction (XRD).

2. Experimental procedures

The material used was an AISI304 austenitic stainless steel plate with a thickness of 1.0 mm under annealed condition, provided by Goofellow Metals Limited, UK. The chemical composition of the steel is in wt%: ~0.08 C, 18 Cr, 10 Ni, 1.4 Mn, and ~0.5 Si [14]. The plate was cut into specimens with a size of 12 mm × 12 mm. The specimens were polished with SiC paper in the sequence 320, 800, 1200, and 2400 grit. All the specimens were heated at a rate of 5°C/minute to 800°C in air, oxidised there for 200 h, and then furnace-cooled to room temperature. After oxidation, the oxidation layer on one side of the specimen was polished off and the exposed metal surface served as one electrode. A platinum foil 0.1 mm × 8 mm × 8 mm in size was placed to the oxide film on the other side of the specimen and acted as the other electrode. In order to improve the contact between the oxide film and the platinum electrode, a uniform pressure of 0.01 MPa was applied to the oxide film during impedance measurements. After the measurements, no additional cracks were found in the oxide surface by observation using SEM. Impedance measurements were made on already oxidised films, which were furnace-cooled to room temperature, connected to electrodes, and subsequently reheated to the measurement temperatures. In this work, three repeat specimens were used for each impedance measurement.

Impedance measurements were made using a Solartron SI 1255 HF frequency response analyser equipped with a Solartron 1296 dielectric interface, controlled by a computer. In the measurements, an AC (alternating current) amplitude of 0.1 V was applied to the specimen with the AC frequency in the range of 1 Hz to 5×10^6 Hz. We have verified that the response with a perturbation of 0.1 V is still linear, even with a perturbation of 0.5 V. To avoid the effect of moisture on the impedance, impedance measurements were performed at temperatures above 100°C. Spectra analysis was carried out using Zview impedance analysis software (Scribner Associates Inc., Southern Pines, NC) to extract the electrical properties of the oxide film.

A JEOL840 scanning electron microscope equipped with an energy dispersive X-ray (EDX) microanalyzer (LINK AN10000) was employed to characterise the microstructure of the oxide film. EDX microanalysis of the matrix and the oxide film surface was carried out in an area analysis mode within an area of 100 μm^2. For each element analysed, the mean value of three data points together with the standard deviation was taken as the measured result. The chemical composition at the surface of the oxide film was determined using a VG ESCALAB 210 XPS under a base pressure of 10^{-9} torr using Mg K_α X-ray radiation (1253 eV) with a power of 200 W. Prior to the surface analysis, the surface was cleaned using argon ion sputtering to eliminate contamination. The crystal structures of the oxide film were determined using XRD.

3. Results

The electrical properties of different oxidised specimens have been measured using impedance measurements. In impedance measurements [8, 12, 15], a sinusoidal potential perturbation is applied to the test electrodes, which is in contact with the electrolyte material to be examined. Impedance diagrams are acquired by measuring the magnitude and phase shift of the resulting current, involving resistive and capacitive responses. As described in Refs. [8, 16, 17], for an oxide scale system, the measured capacitance response is often not ideal, i.e., it does not behave as a pure capacitor. This deviation may be modified by the use of a constant phase element (CPE) for spectra fitting instead of an ideal capacitance element. The impedance of a CPE was given by [8, 16, 17]

$$Z_{\mathrm{CPE}} = \frac{1}{A(j\omega)^n} \tag{1}$$

where A is a fit parameter that is independent of frequency. In the ideal case where the exponential factor $n = 1$, the CPE functions as an ideal capacitor with A equal to the capacitance C. In most cases, n is less than 1. Therefore, the fitting results are represented by A and n. It should be noted that n is just a mathematical factor and has no physical meaning but allows an effective approach to modelling complicated relations among several elements (R, C, etc.) [17]. In general, the CPE is associated with inhomogeneity behaviour, such as surface roughness or porosity, which may cause frequency dispersion. In the case of non-ideal capacitive

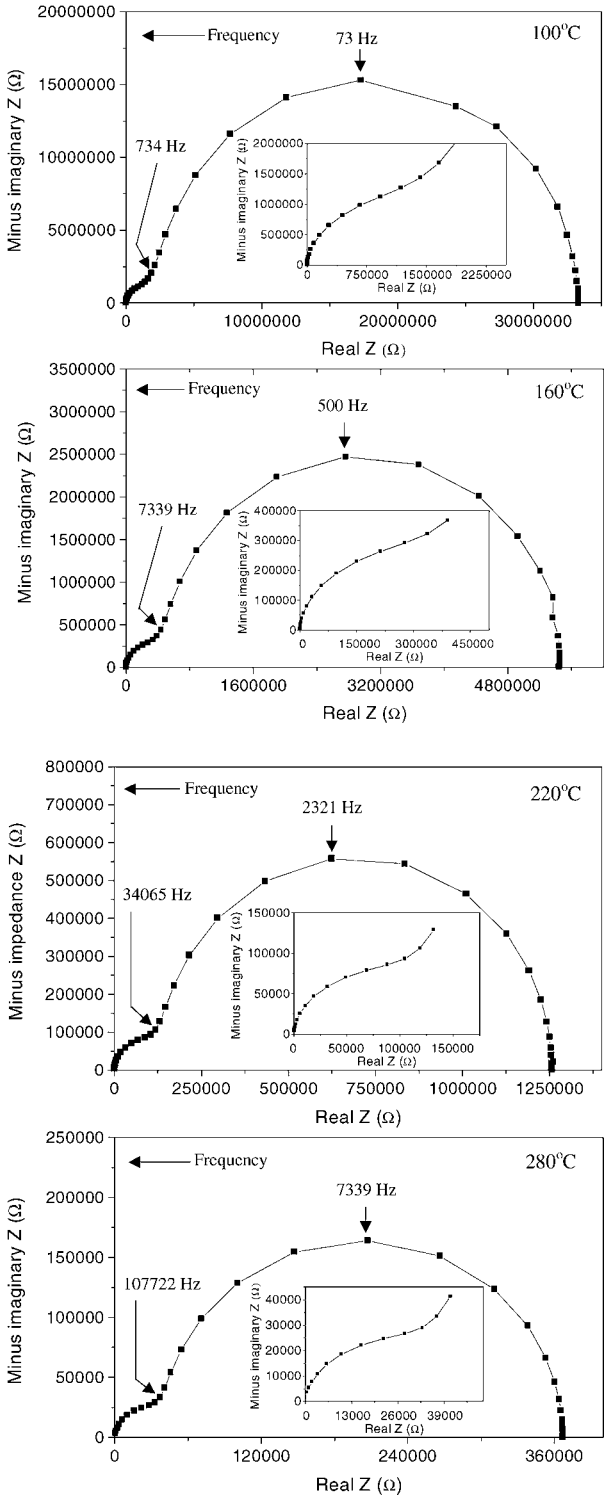

Figure 1 Typical Nyquist plots from impedance measurements at different temperatures with insets showing the high-frequency-range parts.

response mentioned above, the value of A cannot be used to represent the capacitance of the system. Here the capacitance, C, may be acquired by [18]

$$C = R^{(1-n)/n} A^{1/n} \quad (2)$$

where R is the resistance.

Typical Nyquist plots at different temperatures from a specimen are given in Fig. 1. Obviously, there are two semicircles on each Nyquist plot, indicating that two individual oxide layers were produced from the oxidation. These two oxide layers have different electrical and dielectric properties. The resistance of the oxide layers

TABLE I Results from EDX microanalysis of the steel matrix and the oxide film, determined by area analysis (wt%)

Element	Matrix	Oxide film
Fe	70.8 ± 0.1	33.9 ± 1.6 (depleted)
Cr	18.8 ± 0.2	52.1 ± 1.4 (enriched)
Ni	8.5 ± 0.1	3.8 ± 0.3 (depleted)
Mn	1.4 ± 0.1	8.8 ± 0.4 (enriched)
Si	0.6 ± 0.1	1.4 ± 0.1 (enriched)

decreased with increasing temperature, showing a negative temperature coefficient. Typical scanning electron micrographs of the film surface and cross section are shown in Fig. 2. The surface of the oxide film is quite rough. There are no apparent cracks present (Fig. 2a). However, it is impossible to distinguish different oxide layers by examining the cross-section of the oxide film (Fig. 2b). The film thickness is about 1 μm, which is nearly the same as that found in Ref. [12] for the same oxidation time. The EDX results (Table I) show that Cr, Mn and Si are enriched and Fe and Ni are depleted in the oxide film. Since the analysed depth by EDX ($\sim$3 μm [19]) is much larger than the film thickness ($\sim$1 μm), the EDX results also show a contribution from the metal substrate. Therefore, the actual enrichment of Cr, Mn and Si or depletion of Fe and Ni in the oxide film should be much more than that shown in Table I. Fig. 3 shows a typical XRD pattern, indicating the presence of $MnCr_2O_4$ spinel and the Cr_2O_3 phases. There is no peak showing the presence of a Si-containing phase, e.g. SiO_2. However, this does not preclude the existence of SiO_2 with an amorphous form. A typical XPS spectrum from the surface analysis of the oxide film is shown in Fig. 4, indicating that there are Mn, Cr and O with a small amount of Fe present in the surface layer. The quantification based on the spectrum indicates that the surface layer of the oxide contains about 57 at%O, 28 at%Cr, 11 at%Mn, and 4 at%Fe. This layer should therefore be composed of $MnCr_2O_4$ spinel containing a little Fe. According to the XRD and XPS results, Cr_2O_3 should be present beneath the $MnCr_2O_4$ surface layer.

It is worth mentioning that Cr_2O_3, $MnCr_2O_4$, and SiO_2 are all electronic semiconducting oxides and their ionic conduction is negligible [20–22]. Therefore, the electrode–oxide interface is a non-blocking interface and there will be no electrode effect present in the impedance spectra [23], indicating that both semicircles in the spectra stem from the oxide film itself.

4. Discussion

As described in the introduction section, the addition of chromium to high temperature alloys has often been used for producing a protective oxide film [3]. Previous studies of the oxidation of Mn-bearing Cr steels below 900°C [9–11] indicates that when the Cr content is between 17 wt% and 25 wt% the oxide film consists of $MnCr_2O_4$ spinel and Cr_2O_3, where the spinel may contain some Fe. If silicon is present in a high Cr steel, an SiO_2 layer may be formed underneath the outer $MnCr_2O_4$ spinel and Cr_2O_3 layers [3]. The oxidation of a silicon-bearing austenitic stainless steel may

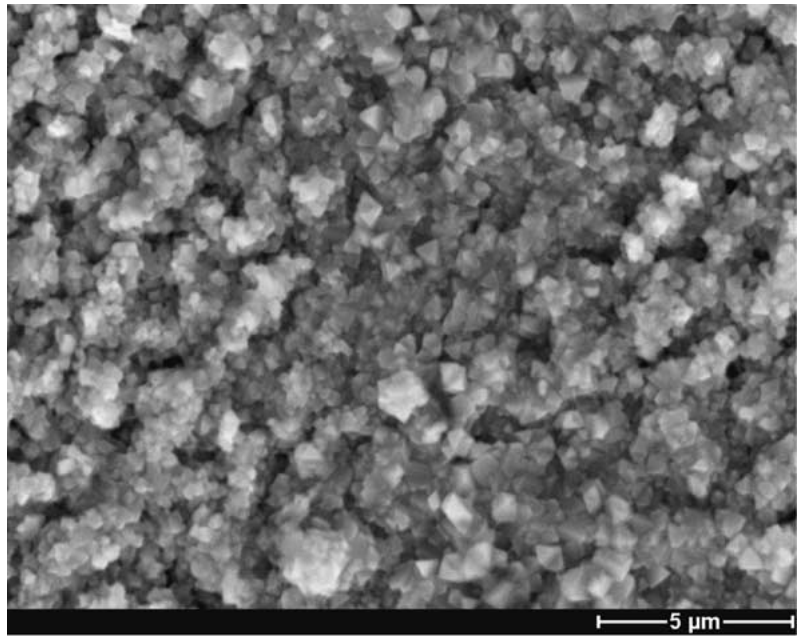

(a)

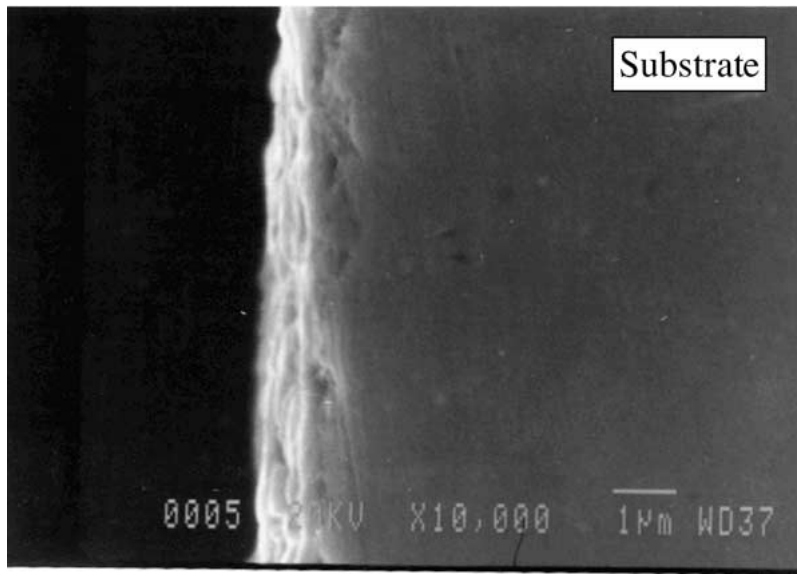

(b)

Figure 2 Scanning electron micrographs of (a) the oxide film surface and (b) the cross section from the oxide surface to the metal matrix.

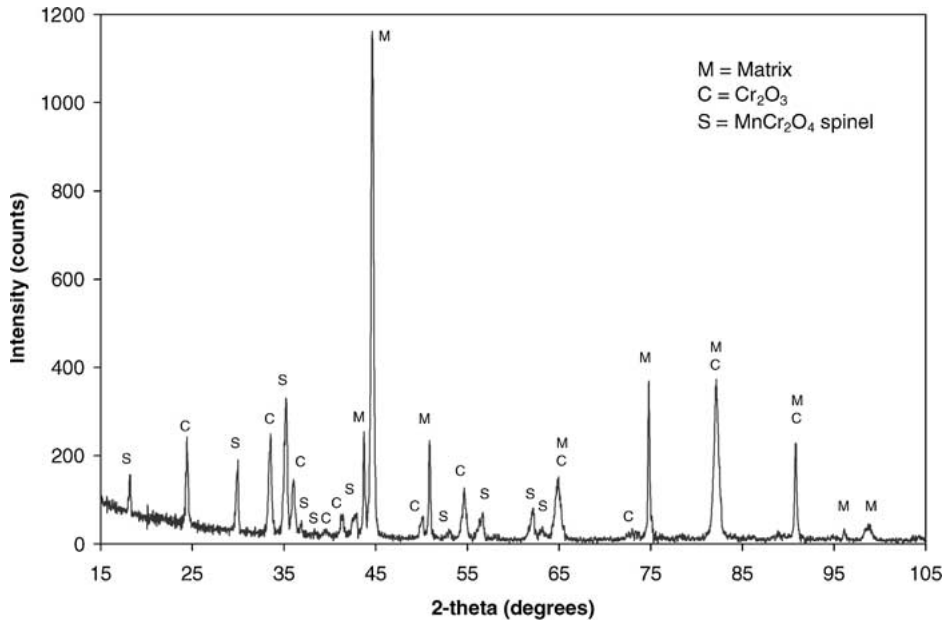

Figure 3 X-ray diffraction pattern from the oxide film along with the steel matrix.

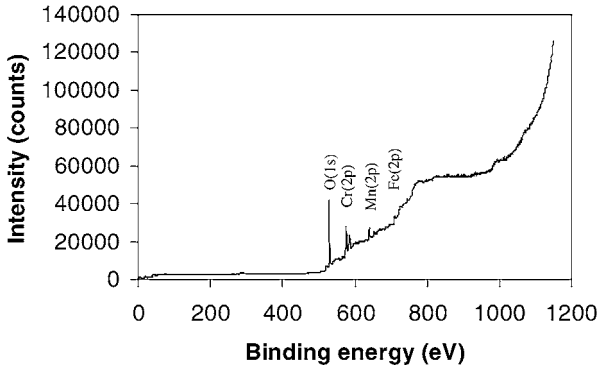

Figure 4 A typical spectrum from the XPS analysis of the oxide film surface.

also lead to the formation of a thin amorphous SiO_2 layer [12, 13]. Of note is that in Ref. [13] when the material was oxidised in air at 700°C for 80 h, the film thickness was about 1.15 μm, indicating a faster oxidation kinetic process than in our case or in Ref. [12]. This might be attributed to Cu as the formed $MnCr_2O_4$ spinel contained apparent Cu.

The XRD data (see Fig. 3) show the presence of $MnCr_2O_4$ and Cr_2O_3 while the impedance results demonstrates the presence of two individual (or independent) oxide layers (Fig. 1). However, the EDX analysis (see Table I) does show the enrichment of Si in the oxide film, suggesting that a possible silica layer may be too thin to be detected by XRD and not sufficiently continuous to be detected using impedance measurements. This cannot exclude the silica existing in an amorphous form. Clearly, these results are generally consistent with those presented in Refs. [3, 12, 13]. In order to relate the two semicircles to the oxides, we need to obtain the electrical and dielectric properties from the impedance spectra. Owing to the fact that two-semicircle impedance spectra are present in the impedance spectra, the spectra may be fitted based on a circuit of two *R*-*C* components with a series connection (Fig. 5a) [8]. In this equivalent circuit, CPE is

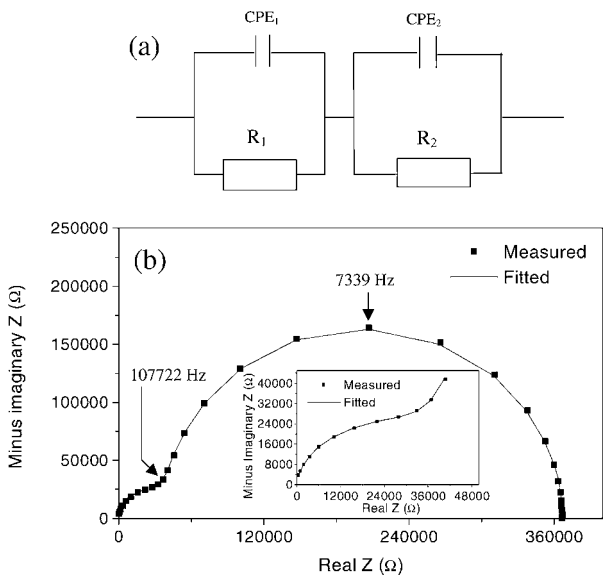

Figure 5 (a) Equivalent circuit model of the oxide film and (b) a typical fitted plot together with the corresponding measured impedance spectrum at 280°C with an inset showing the high-frequency-range part.

the constant phase element as described above. The fitting was performed by virtue of Zview impedance analysis software with the above equivalent circuit. Owing to the fact that the impedance spectra obtained in this work cover a wide range of impedance, in the fitting the data weighting was chosen as Calc-Modulus, which may give a better fit because each data point weight is normalised by its magnitude [24]. A typical fitted impedance spectrum is shown in Fig. 5b, together with the measured one. Evidently, the fitted and measured results match very well with each other, suggesting that the reliable values of R, C and n would be obtained. It should be noted that the oxide film-platinum interface in our study is a non-blocking interface since both materials are electronic conductors [23]. There was no electrode effect at the interface, i.e. there was no semicircle corresponding to the electrode in the impedance spectra. As it can be seen in Fig. 1, the semicircles are not very depressed, i.e. it cannot be due to the roughness at the electrode/oxide interface. The oxidation was controlled by diffusion, which typically produced a multiplayer structure. The analysis of impedance spectra and comparison with previous works indicate that the two semicircles should correspond to the two oxide layers present in the scale. The values of n and capacitance are represented in Tables II and III, respectively, for different specimens. All the n values are above 0.95, demonstrating that the oxide layers behaved, to a large extent, like an ideal capacitor. The capacitance has no apparent variation with measuring temperature. This temperature-independent phnomenon is in line with the work conducted by Fletcher *et al*. for an yttria-stablised zirconia [16]. In addition, the value of capacitance for the low-frequency semicircle is about 5 times as large as that for the high-frequency one. This indicates that the oxide layer corresponding to the low-frequency semicircle may be much thinner than the oxide corresponding to the high-frequency semicircle because the capacitance is inversely proportional to the layer thickness.

The temperature dependence of resistance (R) is represented in Fig. 6 for different specimens. The resistance decreased with increasing temperature. In Fig. 6, $\ln(R)$ is plotted as a function of reciprocal temperature ($1/T$), which shows a linear relationship. Accordingly, the resistance, R, can be expressed as

$$R = R_o \exp\left(\frac{E_\sigma}{kT}\right) \tag{3}$$

TABLE II n values obtained from spectra fitting for different specimens

Temperature (°C)	Specimen 1	Specimen 2	Specimen 3	Mean
	Low-frequency semicircle			
100	0.95	0.98	0.97	0.97
160	0.95	0.97	0.95	0.96
220	0.98	1.00	0.99	0.99
280	0.99	1.00	1.00	1.00
	High-frequency semicircle			
100	0.97	0.97	0.96	0.97
160	0.97	0.95	0.96	0.96
220	0.96	0.96	0.96	0.96
280	0.97	0.95	0.98	0.98

TABLE III Capacitance obtained from spectra fitting for different specimens

Temperature (°C)	Specimen 1	Specimen 2	Specimen 3	Mean
		Low-frequency semicircle		
100	7.00×10^{-11}	9.73×10^{-11}	1.19×10^{-10}	9.54×10^{-11}
160	6.59×10^{-11}	6.30×10^{-11}	8.82×10^{-11}	7.24×10^{-11}
220	6.91×10^{-11}	7.44×10^{-11}	9.14×10^{-11}	7.83×10^{-11}
280	6.35×10^{-11}	6.77×10^{-11}	8.78×10^{-11}	7.30×10^{-11}
		High-frequency semicircle		
100	1.05×10^{-11}	1.10×10^{-11}	8.29×10^{-12}	9.93×10^{-12}
160	1.08×10^{-11}	1.03×10^{-11}	7.95×10^{-12}	9.68×10^{-12}
220	1.02×10^{-11}	1.02×10^{-11}	7.79×10^{-12}	9.40×10^{-12}
280	1.43×10^{-11}	1.08×10^{-11}	8.48×10^{-12}	1.12×10^{-11}

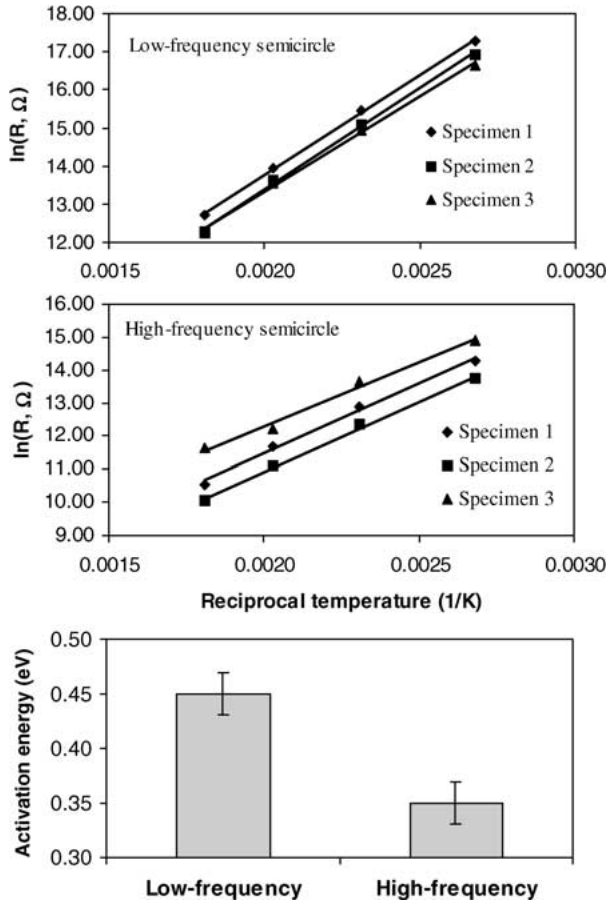

Figure 6 Temperature dependences of resistance (R) for different impedance semicircles and their corresponding activation energies for electrical conduction.

where R_o is a constant depending on both the resistivity and the oxide layer geometry, E_σ is the activation energy for electrical conduction, k is Boltzmann's constant, and T is the absolute temperature. The activation energy E_σ, obtained based on the resistance-temperature relationship, is also shown in Fig. 6. The activation energy for the low-frequency semicircle (~0.45 eV) is apparently higher than that for the high-frequency one (~0.35 eV), implying that the electrical conductivity of the oxide corresponding to the low-frequency semicircle is lower than that to the high frequency semicircle.

The relaxation frequency, f_R, may be obtained from the measured values of R and C according to [8]

$$f_R = \frac{1}{2\pi RC} \tag{4}$$

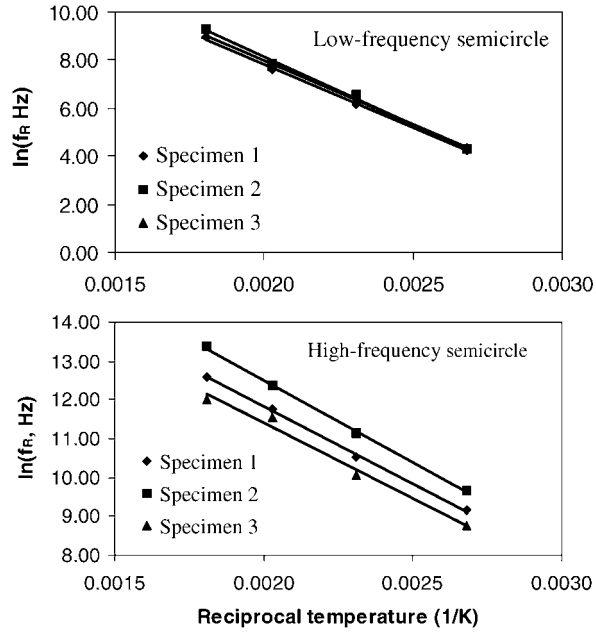

Figure 7 Temperature dependences of relaxation frequency (f_R) for different impedance semicircles.

The relaxation frequency is a material property at a given temperature and independent of the oxide layer geometry. The relaxation frequencies for different specimens, acquired from Equation 4, are represented in Fig. 7 as a function of temperature, indicating a linear relationship between $\ln(f_R)$ and $1/T$. This linear relationship has also been observed in an yttria-stabilised zirconia [16]. As in the case of resistance, the frequency may be expressed as

for the low-frequency semicircle

$$f_R = (1.7 \pm 1.0) \times 10^8 \exp\left[-\frac{(0.45 \pm 0.02)\text{eV}}{kT}\right]\text{Hz} \tag{5}$$

and for the high-frequency semicircle

$$f_R = (6.6 \pm 6.0) \times 10^8 \exp\left[-\frac{(0.35 \pm 0.02)\text{eV}}{kT}\right]\text{Hz} \tag{6}$$

Since the relaxation frequency is independent of the specimen geometry and is a material property at a given temperature, it may be used to identify the material [8, 16]. According to Equations 5 and 6, at room temperature (20°C) the relaxation frequency is about 1 Hz for

the low-frequency semicircle and 600 Hz for the high-frequency semicircle.

Based on the values of conductivity and dielectric constant obtained from literature, the frequency, f_R, may also be calculated by [8]

$$f_R = \frac{\sigma}{2\pi\varepsilon_o\varepsilon} \tag{7}$$

where ε_o is the vacuum permittivity with the value of 8.85×10^{-12} F m^{-1}, ε is the dielectric constant, and σ is the conductivity. The dielectric constants are about 5 for $MnCr_2O_4$ spinel [25], 9.2 for Cr_2O_3 [26], and 3.5 for SiO_2 [26]. The conductivities at room temperature are about 10^{-9}, 10^{-7}, and 10^{-13} Ω^{-1}m^{-1} for $MnCr_2O_4$ spinel [25], Cr_2O_3 [26], and SiO_2 [26], respectively. We can estimate from Equation 7 that the relaxation frequencies are about 3, 2×10^2, 5×10^{-4} Hz for $MnCr_2O_4$ spinel, Cr_2O_3 and SiO_2, respectively. Since a given material has a certain relaxation frequency, the high-frequency semicircle with a relaxation frequency of ~600 Hz at room temperature, which has the same order of magnitude as 2×10^2 Hz, should correspond to the Cr_2O_3 layer and the low-frequency semicircle with a relaxation frequency of ~1 Hz, which has the same order of magnitude as 3 Hz, to the $MnCr_2O_4$ spinel layer. It is reasonable that there is some difference between the calculated values from available data and those from the results obtained in this work because the available data in literature are usually acquired from bulk materials with specific chemical composition and microstructure. In the work by Pan *et al.* [12], the relaxation frequencies corresponding to the semicircles measured from an AISI 304 stainless steel oxidised in air for 1000 h are $\sim 10^{-4}$ for the low-frequency semicircle and $\sim 10^2$ for the high-frequency semicircle. They claimed that the low-frequency semicircle is from the chromia and the high-frequency semicircle from the spinel. However, in terms of the relaxation frequencies estimated from Equation 7, it appears in their case that the low-frequency semicircle stems from the SiO_2 layer rather than the chromia layer and the high-frequency semicircle from the chromia layer rather than the spinel layer. This may be because the electrolyte solution (0.1 M Na_2SO_4) penetrated into the porous spinel to make it short-circuited. This situation is not the case for our work as we used a platinum foil attached to the oxide surface as the electrode. The SiO_2 signals were not detected in the present impedance measurements. This may be because the SiO_2 has not yet formed an independent layer between the Cr_2O_3 and the substrate.

With the provision of capacitance, the film thickness, d, may be calculated by

$$d = \frac{\varepsilon\varepsilon_o A}{C} \tag{8}$$

where A is the electrode area (64 mm^2) and dielectric constant ε_o is 5 for $MnCr_2O_4$ spinel [25], and 9.2 for Cr_2O_3 [26]. The predicted thickness calculated based on the equation 8 is 39.2 μm for the spinel layer and 518.3 μm for the chromia layer. Apparently, the predicted values are much higher than the observed ones (total thickness is ~1 μm). This phenomenon is mainly caused by the poor contact between the foil electrode and the surface of the oxide scale, especially when the surface of the oxide scale is rough. The work by Fletcher, West and Irvine [15] indicates that the effective contact area is less than 1% between the gold foil and the zirconia pellets, resulting in an extremely low capacitance measured by impedance spectroscopy. Assuming that the effective electrode area is 1% of the apparent electrode one, a thickness of ~0.4 μm for the spinel layer and ~5.0 μm for the chromia layer would be obtained. The thickness predicted is still larger than the observed one, but they become reasonable. The impedance measurements mainly predict the presence of two oxide layers in the oxide scale. In addition, it also demonstrates that the thickness of chromia is much larger than the spinel. The impedance spectroscopy study by Pan *et al.* [12] shows that the spinel layer is much thicker than the chromia layer. We believe, in the light of the preceding discussion, that the spinel layer in their case appears to refer to the chromia layer and the chromia layer to the silica layer. It has well been recognised [3] that the silica layer formed on stainless steels during high-temperature oxidation is very thin. The electron microscopy study by Botella, Merino and Otero [13] indicates that the spinel thickness is close to the chromia thickness. However, their oxidation was carried out at 700°C and there was some copper present in the film, which may cause some difference in film structure. In consideration of all the above, it can be concluded that if multioxides in the oxide scales have a laminate structure the impedance spectroscopy can be used to identify them and to determine their relative thickness.

5. Conclusions

The oxide film formed on an AISI304 stainless steel during oxidation in air at 800°C for 200 h was examined by means of impedance spectroscopy in conjunction with scanning electron microscopy, X-ray photoelectron spectroscopy and X-ray diffraction. The film was composed of two independent oxide layers, the outer $MnCr_2O_4$ spinel layer and the inner Cr_2O_3 layer, together with an incomplete SiO_2 layer underneath them. The $MnCr_2O_4$ spinel layer was apparently thinner than the Cr_2O_3 layer. The activation energies for electrical conduction are experimentally determined as about 0.45 and 0.35 eV for the $MnCr_2O_4$ spinel and Cr_2O_3 layers, respectively.

Acknowledgements

This work was supported by EPSRC (UK) under grant no. GR/M86743. The authors would like to acknowledge Prof. Brian Ralph for commenting on the manuscript.

References

1. M. F. DAY, "Materials for High-Temperature Use" (Oxford University Press, Oxford, UK, 1979).
2. J. K. TIEN and T. CAULFIELD, "Superalloys, Supercomposites and Superceramics" (Academic Press, New York, USA, 1989).

3. M. SCHUTZE, "Protective Oxide Scales and Their Breakdown" (John Wiley and Sons, Chichester, UK, 1997).
4. N. BIRKS and G. H. MEIER, "Introduction to High Temperature Oxidation of Metals" (Edward Arnold, London, UK, 1983).
5. S. SHIBAGAKI, A. KOGA, Y. SHIRAKAWA, H. ONISHI, H. YOKOKAWA and J. TANAKA, *Thin Solid Film* **303** (1997) 101.
6. A. DIAS and V. D. F. C. LINS, *Corrosion Sci*. **40** (1998) 271.
7. S. SEAL, R. NARDELLI, A. KALE and V. DESAI, *J. Vac. Sci. Technol*. **A17** (1999) 1109.
8. J. R. MACDONALD (ed.), "Impedance Spectroscopy" (John Wiley & Sons, Chichester, UK, 1987).
9. H. J. YEARIN, H. E. BORN and R. E. WARR, *Corrosion* **12** (1956) 561.
10. H. J. YEARIN, W. D. DERBYSHIRE and J. F. RADAVICH, *Corrosion* **13** (1957) 597.
11. G. C. WOOD, T. HODGKIESS and D. P. WHITTLE, *Corrosion Sci.* **6** (1966) 129.
12. J. PAN, C. LEYGRAF, R. F. A. JARGELIUS-PETTWEAAON and J. LINDEN, *Oxid. Met*. **50** (1998) 431.
13. J. BOTELLA, C. MERINO and E. OTERO, *Oxidation of Metals* **49** (1998) 297.
14. Goodfellow Catalogue 2000/2001 (www.goodfellow.com) (Goodfellow Metals Limited, Ermine Business Park, Huntingdon, UK, 2000).
15. S.-H. SONG and P. XIAO, *Scripta Mater.* **44** (2001) 601.
16. J. G. FLETCHER, A. R. WEST and J. T. S. IRVINE, *J. Electrochem. Soc*. **142** (1995) 2650.
17. S. T. AMARAL and I. L. MULLER, *Corrosion* **55** (1999) 17.
18. T. JACOBSEN, B. ZACHAU-CHRISTIANSEN, L. BAY and S. SKAARUP, in Proceedings of the 17th Riso Internaltional Symposium on Materials Science, "High Temperature Electrochemistry: Ceramics and Metals," edited by F. W. Paulsen, N. Bonanos, S. Linderoth, M. Mogensen and B. Zachau-Christiansen (Riso National Laboratory, Roskilde, Denmark, 1996) p. 29.
19. S. J. B. REED, "Electron Microprobe Analysis" (Cambridge Univ. Press, Cambridge, UK, 1975).
20. O. KUBASCHEWSKI and B. E. HOPKINS, "Oxidation of Metals and Alloys," 2nd ed. (Butterworths, London, 1967).
21. Y.-M. CHIANG, D. P. BIRNIE and W. D. KINGERY, "Physical Ceramics" (John Wiley & Sons, New York, 1997).
22. A. M. ALPER, "High Temperature Oxides, Part 1: Magnesia, Lime and Chrome Refractories" (Academic Press, New York, 1970).
23. R. D. ARMSTRONG and M. TODD, in "Solid State Electrochemistry," edited by P. G. Bruce (Cambridge University Press, Cambridge, UK, 1995).
24. Zview for Windows: Impedance/Gain Phase Graphing and Analysis Software–Operating Manual, Version 2.1 (Scribner Associates, Southern Pines, NC, USA, 1998).
25. S.-H. SONG and P. XIAO, unpublished work.
26. G. V. SAMSONOV (ed.), The Oxide Handbook, 2nd ed. (IFI/Plenum, New York, 1982).

Received 20 February
and accepted 24 September 2002